

Spectral optimization of CPV for integrated energy output

Mark McDonaldⁱ and Chris Barnesⁱⁱ

ABSTRACT

The series electrical nature of the multi-junction solar cell is both the source of its desirable overall efficiency and of its sensitivity to spectral balance. Owing to the series connection of the spectrally selective junctions, variations in the spectra of the solar input, optical transfer function, and cell quantum efficiency have significant impact on annual energy production despite being effectively indistinguishable in instantaneous power output. This paper will outline spectral filtering approaches for experimental characterization, and spectral simulation methods for estimating annual energy production. We will also present system level design to optimize for annual energy production.

Keywords: Concentrator Photovoltaic, CPV, current balance, spectral filtering, fill factor, spectral optimization

1. ESTIMATION OF THE SPECTRAL TRANSFER FUNCTION

The series electrical nature of the multi-junction (MJ) solar cell is both the source of its desirable overall efficiency, and of its sensitivity to spectral balance. By design, the photocurrent generated by the higher bandgap junctions is approximately balanced for standard illumination at the level of the solar cell. The MJ cell cost is substantially greater than for more traditional cells, with one major supplier having discussed a 2010 roadmap leading to \$70k per square meterⁱⁱⁱ starting from a 2007 value of ~\$150k per square meter (1). Cost-effective terrestrial solar power generation with present day commercial MJ cells must therefore entail high concentration optics (2). While any optical concentrator would suffer insertion loss, the low cost optics needed to assure cost-effective power generation face tradeoffs that can significantly deviate from ideal. These non-unity spectral transfer functions (STFs) can unbalance the junctions and constrain photocurrent production under standard illumination as well as during field operation.

The 0.5 MW SolFocus optical system installed for ISFOC consists of five STF relevant optical elements: the protective cover glass, a second surface primary mirror, a first surface secondary mirror, a lightguide, and a thin layer of cell encapsulant. Figure 1 shows a side view of the optical system for an individual power unit.

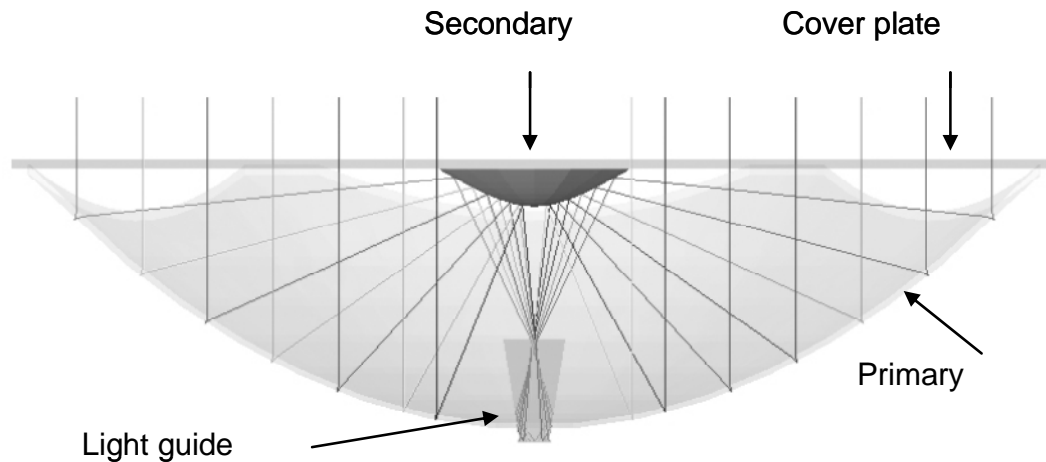


Figure 1 SolFocus optical layout

ⁱ SolFocus Inc., Mountain View, CA, email correspondence mark_mcdonald@solfocus.com

ⁱⁱ Palo Alto, CA

ⁱⁱⁱ Per values in reference 1, 0.35 \$/W at concentration yielding 50W/cm² incident on a cell with 40% efficiency

Each component has a spectrally dependent loss owing to Fresnel reflections, absorption, and optical coatings. The STF function for representative samples of each element was measured in Perkin-Elmer 950 spectrophotometer. The spectrophotometer presents each sample with a rectangular beam measured to be approximately 5 mm by 10 mm, with an input range of angular components measured to be approximately +/-35 mrad vertically and +/-6 mrad horizontally. The transmission measurements are conducted near normal incidence, and the reflection measurements at approximately 8 degrees from normal incidence. The transmission and reflection responses are collected by an integrating sphere.

There is a potential for bias when applying the measured data to the final device owing to the incongruence of the measurement conditions and the use in concentrator optics. A first potential bias arises from the use of an integrating sphere to collect signal for detection. The property of an integrating sphere is that large angle scatter will be included in the signal by the test instrument, but the same large angle scatter would not reach the cell in the final high concentration solar module. In practice, this is not a substantial bias as the components in the SolFocus concentrator have been constructed from highly specular materials (e.g., float glass) and utilized conformal coating processes (e.g., wet chemistry metallization), thus providing substantially smaller angular uncertainty from scatter than the input angular range of the instrument. A second potential measurement bias arises by extrapolating module insertion loss from the near normal incidence measurement of each component to the use condition with incident angles for some rays surpassing 45 degrees. In practice, the variation in silver reflectivity for average polarization is less than 0.25% worst case, and the variation in air/glass interface transmission is less than 1% (see Figure 2). As a weighted average of all ray paths, the system efficiency impact is substantially reduced compared to those modest worst case effects. Hence, we do not anticipate significant bias on the scale of the instrument accuracy arising from either the measurement at normal incidence or hemispherical detection.

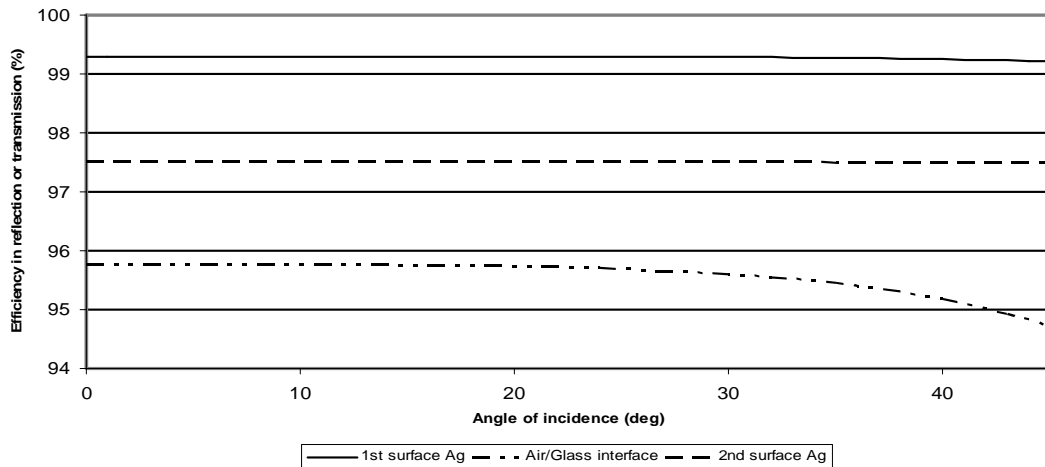


Figure 2 Angular dispersion of the transmissivity of an air/glass interface and reflectivity of silver reflectors

For each of the components, and for the system comprising those components, a normalized STF is shown in Figure 3 and Figure 4 respectively. While the base material of the lightguide is the well-known BK7 glass, the catalog values for absorption and refractive index are spectrally sampled only sparsely at spectroscopic lines (4). Decomposition of the Fresnel reflection and internal transmittance of the lightguide was determined by regression from measurements of the BK7 base material in three different thicknesses of 3 mm, 10 mm, and 50 mm. The estimate for the path length of the final device is shown. The BK7 glass of the lightguide shows an absorption profile suggesting hydroxyl absorption (an increasing insertion loss as for wavelengths greater than 1600 nm and an overtone at ~1385 nm). That suggests that the IR depletion would affect only the bottom junction, which is expected to be in substantial surplus (1). The encapsulant material is a less well documented material. For that reason, the absorption of the encapsulant was obtained by regression by evaluating thicknesses of <0.1 mm, 5.5 mm, and 7 mm contacted by glass plates. The estimate for the path length of in the final device is shown. The encapsulant exhibits several absorption peaks (including one in the vicinity of the hydroxyl overtone), but all such features are for wavelengths >1150 nm, and would affect the bottom junction. The cover glass is a low iron float glass, and exhibits a broad absorption characteristic

from residual iron (3) at ~1200 nm resulting in ~4% peak insertion loss. A similar absorption characteristic is present in the primary mirror, due to the second surface nature of that reflective component, and utilization of a low iron float glass as a substrate. There is a dip in the reflectivity of the secondary mirror in approximately the same spectral region as the primary and the cover plate; however, as this is a first surface mirror, residual iron absorption is not the cause. Instead, this is a result of the thin film nature of the protective coatings applied to the silver reflector. These layers are chosen for protection but are optimized to constructively interfere with the main silver reflection for short visible wavelengths, and add to reflectivity in that band. The interference must necessarily be destructive at somewhat longer wavelengths, reducing reflectivity for a band of longer wavelengths. Much of the effect from the losses peaking near 1200 nm will affect the bottom junction; however, the bandwidth is sufficient that the middle junction will also be affected.

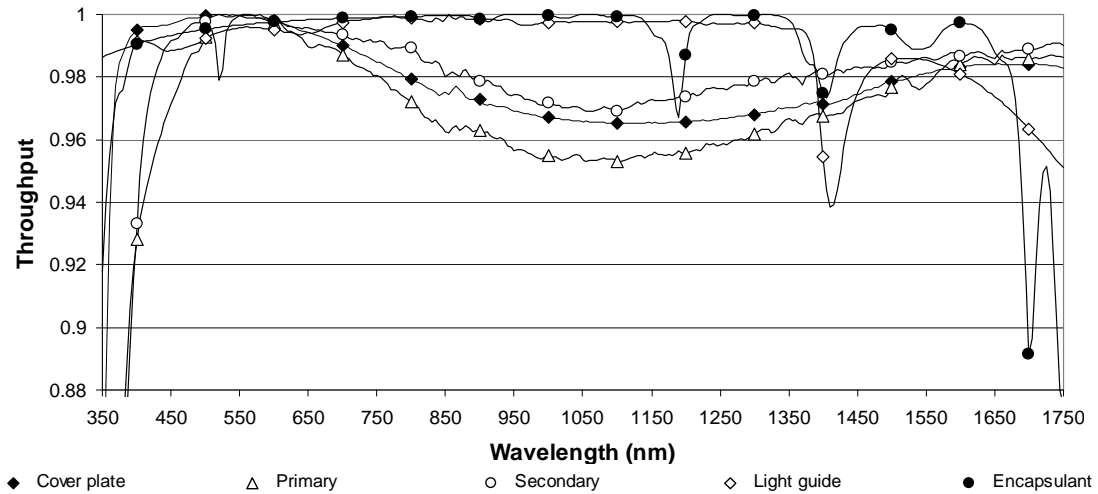


Figure 3 Normalized STF for SolFocus concentrator components

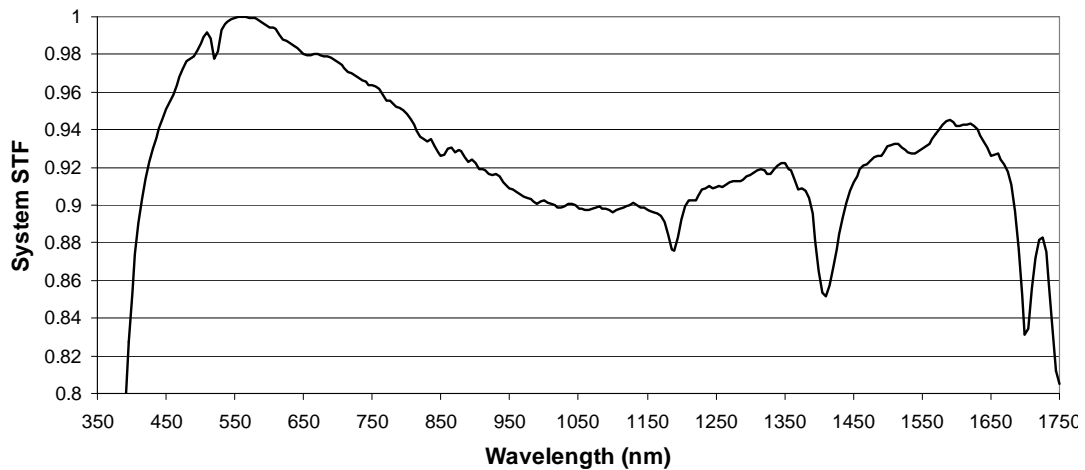


Figure 4 Normalized STF for SolFocus concentrator

2. SPECTRAL MODEL

The goal of this work is to arrive at a predictively useful spectral model of electrical power generation, so that system engineering and tradeoff analysis can be conducted rapidly. We simplify the model by considering a single concentrator power unit, and taking the voltage at maximum power to be essentially unperturbed by the relatively small changes in photon flux. This latter assumption can be justified by observing that the maximum power voltage is slowly varying at concentrations at the cell near 500 (5). These assumptions allow the optimization task to be limited to that of maximizing photocurrent. The optimization is strongly driven by the MJ cell construction. In particular, we model this as 3 photodiodes in series, for which each cell responds to a target slice of the solar spectrum. The external quantum efficiencies (EQEs) for each of the 3 junctions of a commercial MJ cell (5), superimposed on the reference air mass 1.5 direct normal incidence (AM1.5D) spectrum is shown in Figure 5. The 50% level for the top and middle junction EQE has been indicated as an approximate band edge.

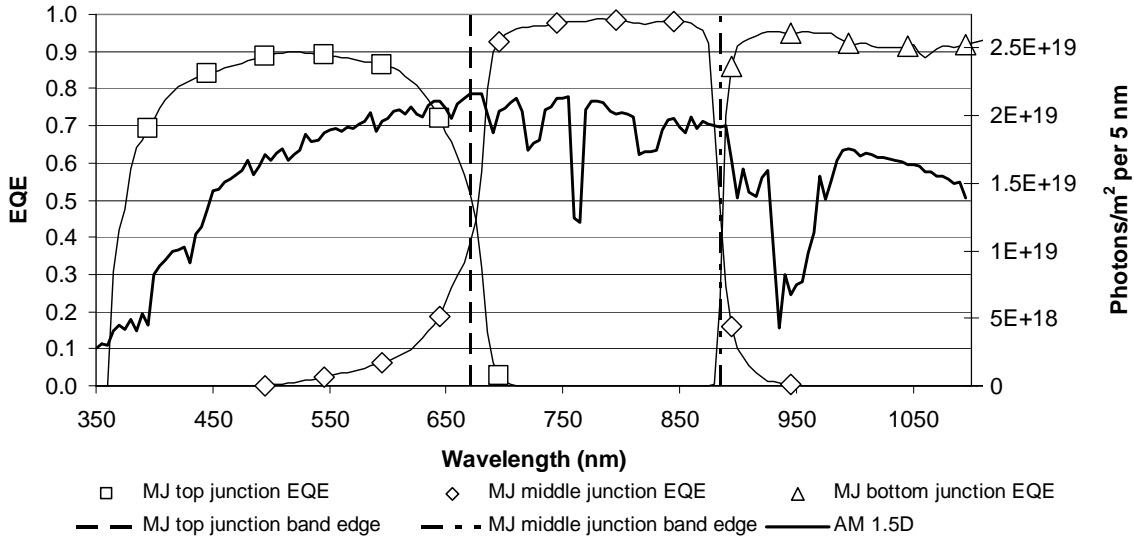


Figure 5 EQEs for each of junction of a commercial MJ solar cell, and AM1.5D spectrum

The 3 junctions will see photo-generation according to

$$J_i = \sum_{\lambda} P(\lambda) \cdot \frac{\lambda}{hc} \cdot STF(\lambda) \cdot EQE_i(\lambda), \quad i = 1, 2, 3$$

where J_i is the photocurrent for the i^{th} junction, $P(\lambda)$ represents the power spectrum input to the concentrator, $STF(\lambda)$ is the spectral transfer function, and $EQE_i(\lambda)$ is the junction specific EQE. The diode response to this input depends on the applied load and is represented generally by an IV curve, and the precise determination of the current for the series connected device of 3 junctions would require an evaluation of the sum of those IV curves. To render the analysis amenable to rapid tradeoff analysis, we choose to approximate the electrical response as the minimum current of the three diodes.

3. EXPERIMENTAL VERIFICATION OF THE SPECTRAL MODEL

The key value we seek for this spectral model approach is predictive accuracy for spectral optimization. We now will test model predictions against corresponding optical hardware using three experimental methods. First, we will compare the system response in experiment and simulation to spectral dependent attenuation imposed by known filters. Second, we will compare the simulated and experimental system response to spectral shifts resulting from changes in solar elevation. Third, we will assess the response of the model and system when assuming an isotope cell as a receiver.

The SolFocus optics provide only limited kaleidoscopic mixing at the cell of the entrance aperture. Moreover, the lateral current spreading in commercial MJ solar cells is limited. For those reasons, sub-aperture filtering would lead to spatially varying spectra, and more difficult to interpret results. We therefore seek a set of filters that can cover the entire SolFocus entrance aperture ($\sim 700 \text{ cm}^2$). To further simplify the analysis of the data, we also seek a set of filters that provide substantial, but diverse, filtering applying to one junction of the MJ cell, but having limited effect on the potential photocurrent of the other junctions. Serendipitously, present day, commercial MJ cells have a top junction bandwidth essentially matched to the human visual response. As a result, there is an extensive library of inexpensive, large area color filters for theatrical lighting applications (Figure 6) that are designed not to have significant heat absorption. These filters meet our needs for controlled depletion of photons that would be absorbed by the top junction.

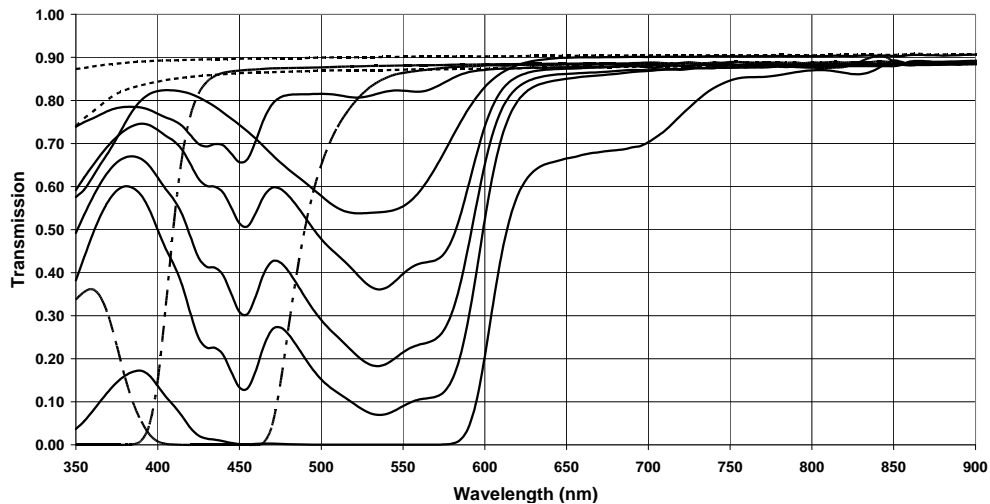


Figure 6 Spectral Transmissivity of Selected Theatrical Lighting Filters

Each of these filters can be multiplied with the concentrator optics spectral transfer function to obtain a new overall system spectral transfer function. The model then applies the solar input, cell EQEs, and reports the simulated photocurrent. This same configuration can then be tested on-sun, and resultant photocurrent recorded.

As an initial experiment, we simulated and measured system response under clear skies for an autumn late afternoon. Under these conditions, the photocurrent would typically be constrained by the top junction (1). Using a subset of filters that are computed to have increasing levels of differential depletion of the spectral band corresponding to the top junction should produce linearly decreasing levels of experimental photocurrent. The comparison of the simulated and experimentally observed result is shown in Figure 7. We observed a high correlation to a linear fit, with a slope near unity and an intercept near zero. The deviation from an ideal slope of 1, and an intercept of 0, suggest absolute accuracy errors of $\sim 5\%$; however, the low scatter around the fit suggests the model is highly predictive.

As our goal is a model supporting spectral optimization of a power unit, the most critical test of the simulation model is to predict transitions of constraint from a first given junction to a second given junction. As our set of filters provides mainly differential depletion for the top junction, we conducted our experiment under an occasion for which middle junction limited cell response is anticipated. For this case, we would expect differential depletion of visible light to have negligible impact on power unit performance to a threshold value of differential depletion beyond which the power unit response will decrease linearly. The comparison of simulated and experimental results is shown in Figure 8. A depiction of the deviation from best fit of top and middle junction limited responses is shown in Figure 9. By inspection, there is a high confidence classification for predictions of junction balance to about 1%. For the set of filters identified as middle junction limited under the expected experimental conditions, the standard deviation in measured normalized power is 0.4%. In sum, the model demonstrates good predictive power both of the form of the response, and critically to the threshold at which the power unit and filter system optimally matches top and middle junction photocurrents.

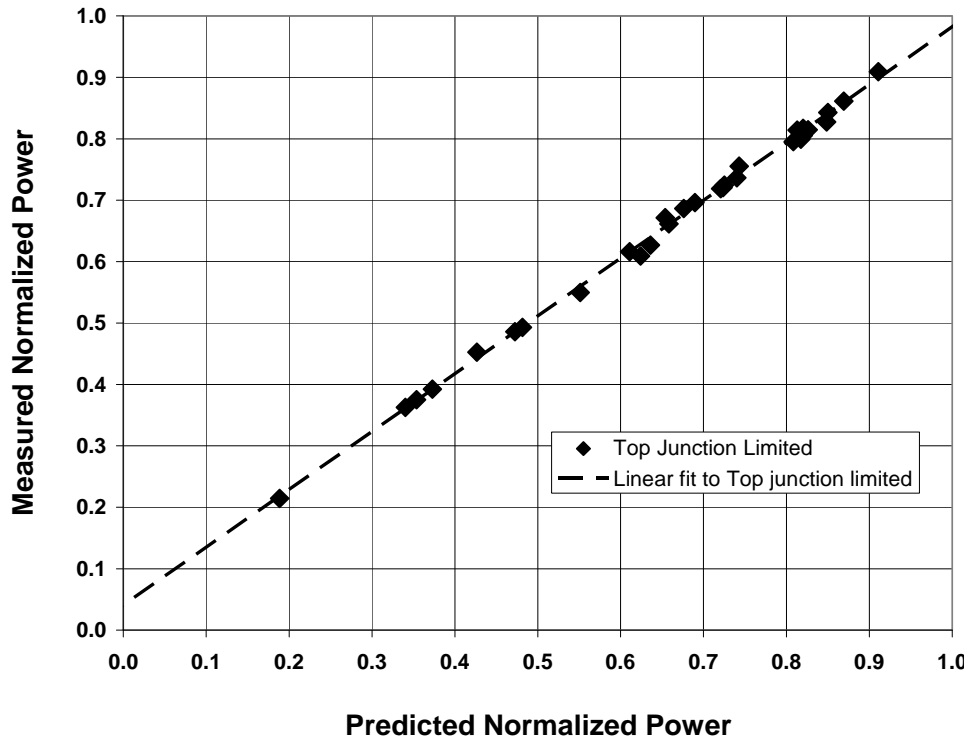


Figure 7 Plot of simulated and experimental normalized power unit photocurrent under conditions of top junction current constraint. Data collected at solar elevation of 20 degrees in late October.

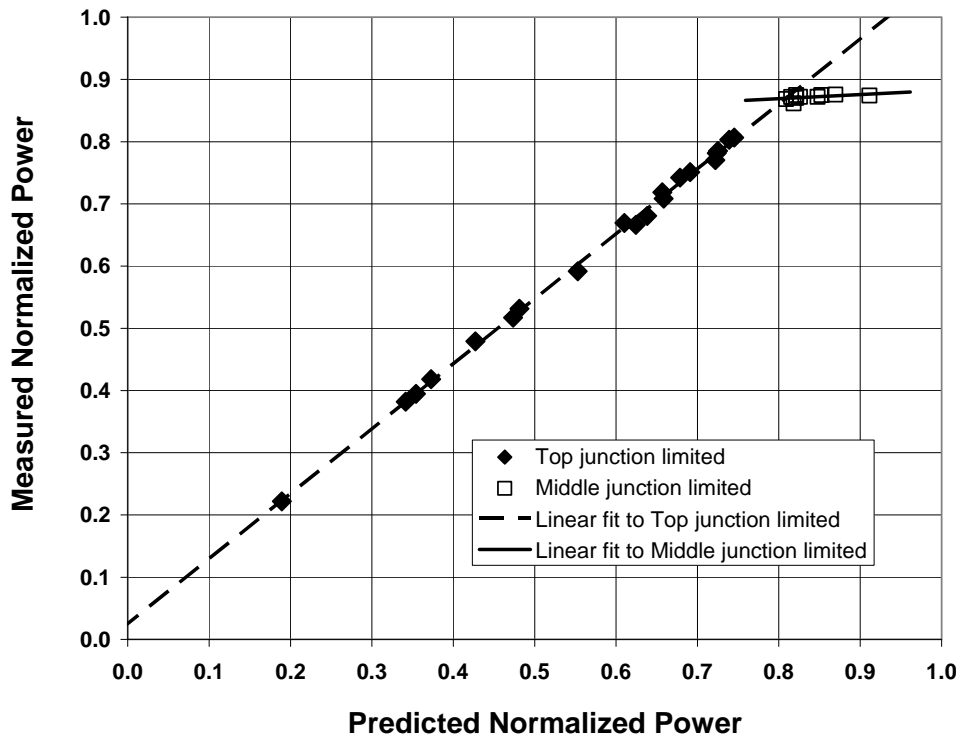


Figure 8 Plot of simulated and experimental normalized power unit photocurrent across threshold of top and middle junction constraints. Data collected at solar elevation of 40 degrees in late October.

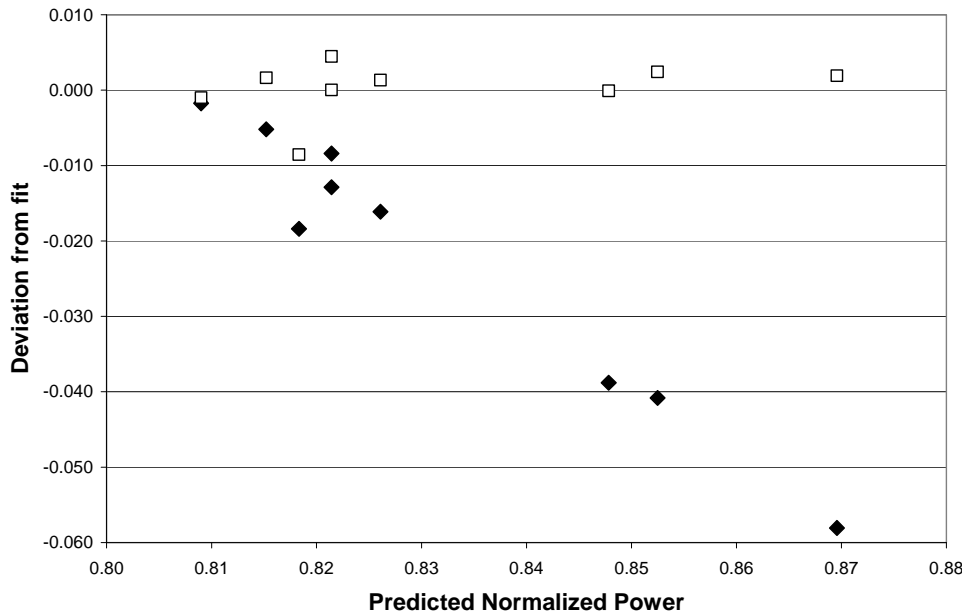


Figure 9 Deviation of measured normalized power from best fits shown in Figure 7, for the filters identified in experiment as middle junction limited.

The above validation method has substantial merit as it utilizes readily available, inexpensive materials, can be applied straightforwardly, and can test the model's robustness against spectral changes with significantly more granularity than the junction bandwidths of the present day commercial cells. Nonetheless, as we intend this model to support high value engineering and manufacturing, we chose to validate the model using two additional methods previously documented in the literature. The first of those methods is the use of fill factor as a direct diagnostic of the photocurrent balance, the second is use of isotype cells which are specially constructed MJ cells that provide photocurrent proportional to one junction only.

Fill factor is a useful diagnostic in that it refers implicitly to the junction photocurrents incorporating all spectral effects, does not require contemporaneous DNI (direct normal irradiance) for interpretation of results, and the minimum achieved at best-current matching provides a relatively sharp feature for precise determination (6). Moreover, the variation in solar spectrum across the course of the day, from relatively depleted in visible light near sunrise and sunset, to relatively rich in visible light near solar noon, incorporates a substantial fraction of the spectral variation that can be anticipated at a given site. Fill factor can be inconvenient in that use of varying solar elevation as a filter requires substantially clear skies throughout the course of a day long measurement.

We collected IV curves throughout a day^{iv} to establish the solar elevation for which the power unit produced a minimum in fill factor, which we found to be ~31 degrees. On a subsequent day, we again collected fill factor throughout the course of a day, and at solar elevations below (substantially top junction limited), slightly above (marginally middle junction limited), and substantially above this threshold solar elevation (substantially middle junction limited). For each of those pre-determined occasions, we conducted a short sequence of experiments with spectral filtering to confirm that the fill factor and spectral filtering method would match to the spectral model prediction. The results of those experiments are shown in Figure 10. The spectral filtering sequence demonstrates a linear response to increasing differential depletion, in agreement with the fill factor analysis. For a solar elevation slightly above the threshold of current matching conditions identified by the fill factor method, we found a linear response to differential depletion with the exception of one filter with very weak depletion, again in agreement with the spectral filtering method. Finally, for a solar elevation substantially above the threshold for which fill factor records a minimum, we find a regime of differential depletion of up to 5% before changing the system behavior from middle junction limited to top junction limited. In each of these cases, we find good qualitative correlation of these methods

^{iv} The gap in data collection was due to shading on the test equipment from a building adjacent to the test equipment.

regarding photocurrent imbalance, and good agreement regarding the identification of the threshold at which the photocurrents are balanced.

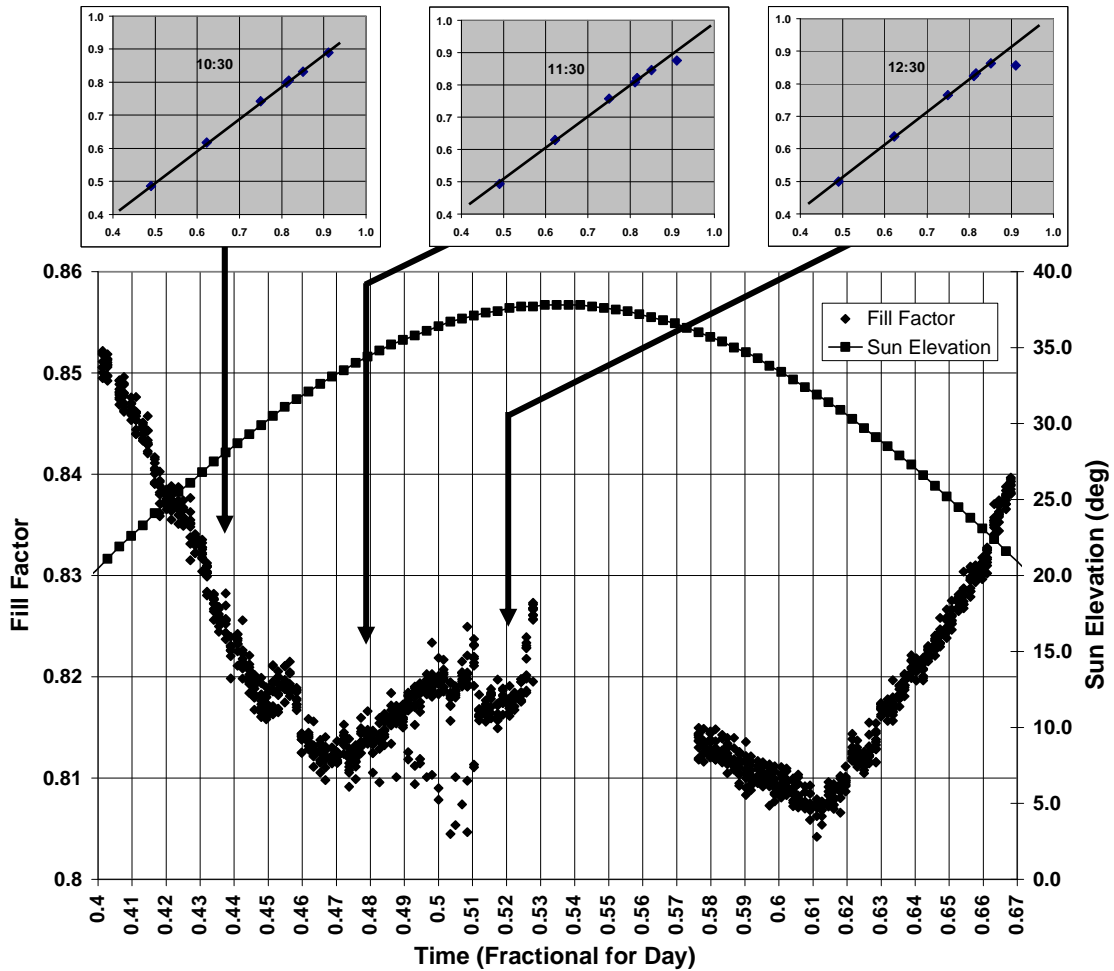


Figure 10 Main chart of fill factor throughout an autumn day, inset charts showing results of spectral filtering at times prior to, near the minimum of, and after the minimum in fill factor

Isotype cells have internal structure identical to MJ cells, but have modified doping profiles to assure that only one junction serves to generate photocurrent. By providing responses related only to a single junction, the experimental impact of the spectral transfer function and solar spectrum can be observed (7), and predictions of the spectral model for each junction can be directly compared. The specific isotype cells used in our work were procured from Spectrolabs. Owing to the altered doping profiles, we anticipated that the isotype EQE responses might differ from the datasheet performance for the corresponding commercial MJ cells. To avoid any significant impact to model accuracy, EQE data was collected for each of the J1 (highest bandgap), and J2 (middle bandgap) isotype cells. The comparison of published response for the MJ cell to that for the isotype cells of the batch used for this work is shown in Figure 11. The most significant difference is the reduced peak EQE of the J2 isotype cell, as compared to the supplied datasheet for the middle junction of the MJ cell. Owing to the approximately 10% difference in terms of determining current balance, we will use the experimental values for the isotype cells where applicable rather than the datasheet EQE values pertaining to the standard MJ cells.

J1, J2, and J3 isotype cells produced from the same batch as those measured for Figure 11 were then assembled into SolFocus concentrator power units. As a reference, we collected data with a power unit assembled with a standard MJ cell. Results of that measurement are shown in Table 1. Note that J_{ratio} is the ratio of the top junction, or J1, photocurrent to the middle, or J2 junction, photocurrent.

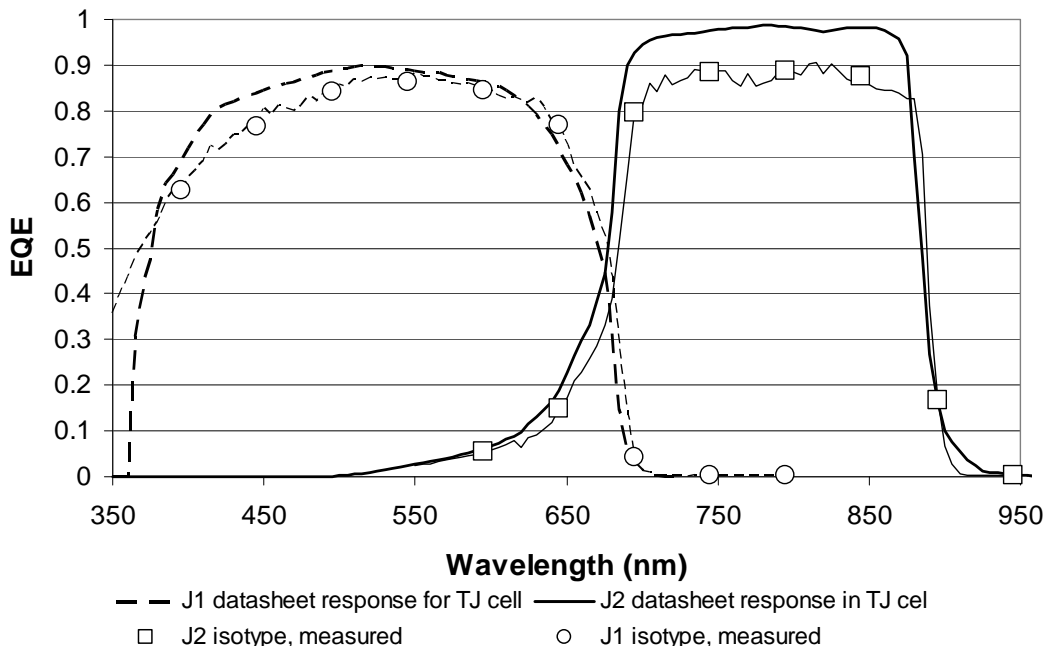


Figure 11 Comparison of datasheet EQE for individual junctions in MJ cell, and EQE of isotype cells used in this work.

Cell	Time	Date	Solar Elevation (deg)	DNI Irradiance (W/m ²)	Short circuit photocurrent, normalized to J2 isotype
Triple junction	1:20	9/27/2007	50.58	971	1.02
J1 isotype	1:27	9/27/2007	50.35	969	1.12
J2 isotype	1:32	9/27/2007	50.15	969	1.00
J3 isotype	1:37	9/27/2007	49.91	968	1.22

Table 1 On-sun measurements of SolFocus concentrator power unit equipped with a commercial triple junction cell, and isotype cells.

Ideally we would have high resolution DNI spectra contemporaneous with the isotype data for model validation purposes. Unfortunately, that data was not available. Absent contemporaneous DNI spectra, we utilized the AM1.5D spectrum to compute the response of the MJ, J1 isotype, and J2 isotype cells (Table 2).

Cell	J _{ratio}
MJ	1.02
Isotype	1.09

Table 2 Computed system J_{ratio} for commercial triple junction cell, and for isotype cells.

As a comparison, the model predicts a J_{ratio} of 1.09 for isotypes against an experimental observation of 1.12, and the model predicts a J_{ratio} of 1.02 against an experimental observation of 1.02.

In summary, we find good predictive value of our spectral model for current balance after experiments of spectral filtering, fill factor, and isotype cells. With the confidence accumulated, we will now proceed to use the spectral model to optimize our system STF.

4. STF OPTIMIZATION

Given a predictive system model, STF optimization requires a training set of input spectra, an understanding of available design freedoms, and a figure of merit. For a figure of merit, we will choose aggregate short circuit photocurrent. This figure of merit is only approximately a measure of system performance, but demonstrates the value of the system optimization approach. As a study of design freedoms, we will consider optimization of the peak wavelength of a commercial AR (anti-reflective) treatment in use for flat plate PV modules (8). A sampling of the family of curves realizable with changes to the resonance wavelength of a double sided porous anti-reflection treatment is shown in Figure 12. The change in peak wavelength was effected by changes in the physical thickness of the porous layer.

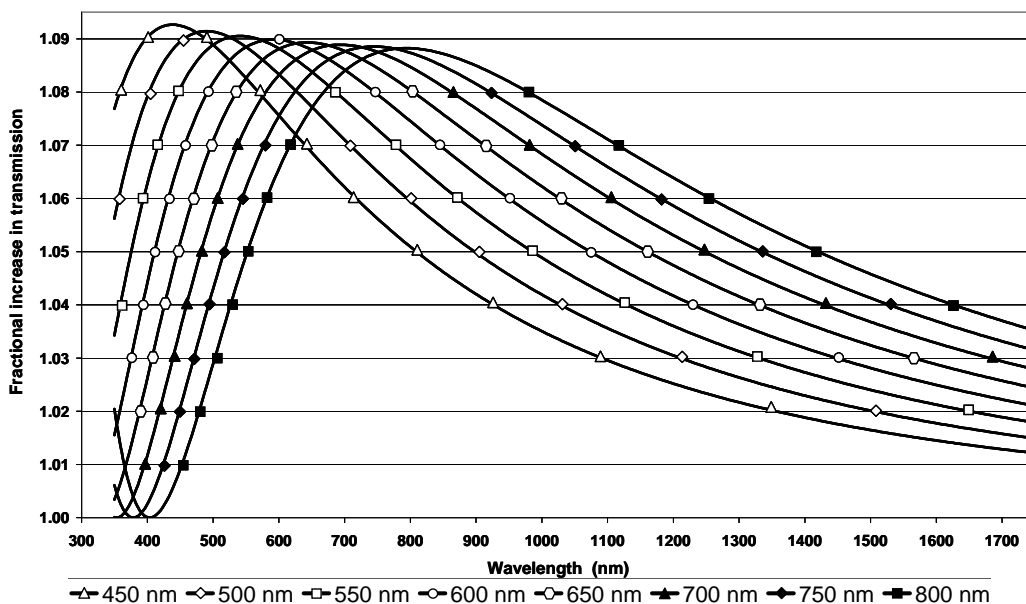


Figure 12 Proportional increase in STF due to cover plate AR, for various peak wavelengths

The spectral model includes this AR as a spectral filter, albeit as a filter with transmission greater than unity. The potential benefit of the AR is evident, with gains in peak transmission of up to ~9%; however, the AR has a finite pass band. Given that the change of thickness of the porous layer is effectively cost-free over the range simulated, the cost-effectiveness of the system will be maximized when the performance figure of merit is maximized.

The remaining modeling choice is that of the input solar spectra. AM1.5D is a traditional choice of reference spectrum for CPV, a single spectrum that represents a range of solar elevations for latitudes and weather conditions of economic interest for CPV. While AM1.5D is a reasonable choice of a typical DNI spectrum, there is no compelling reason that a training set of spectra could not be used to more accurately represent the conditions for a site or sites of particular interest. Indeed, given the non-linear nature of the spectral model, it is fundamentally more accurate to apply any averaging to the output computed photocurrents rather than to the input solar spectrum. The approach of diverse input spectra has been adopted in some recent publications (1), but the spectra used were the product of an atmospheric transfer simulation rather than experimental DNI spectra. As a result, the weather cross-correlated effects of atmospheric variation are imperfectly represented. While use of experimental DNI data has general limitations due to sampling, we opt for the use experimental data to more accurately optimize for a given site.

MJ based CPV is relatively novel, and there is a limited amount of site specific DNI spectra available. We utilized NREL's (and its forerunner SERI's) Spectral Solar Radiation Database for sites in Cape Canaveral, FL and San Ramon, CA (9). From this database, we selected approximately 250 DNI spectra as training sets. A few selected examples from the spectra training set for San Ramon, CA used in the simulation are shown in Figure 13.

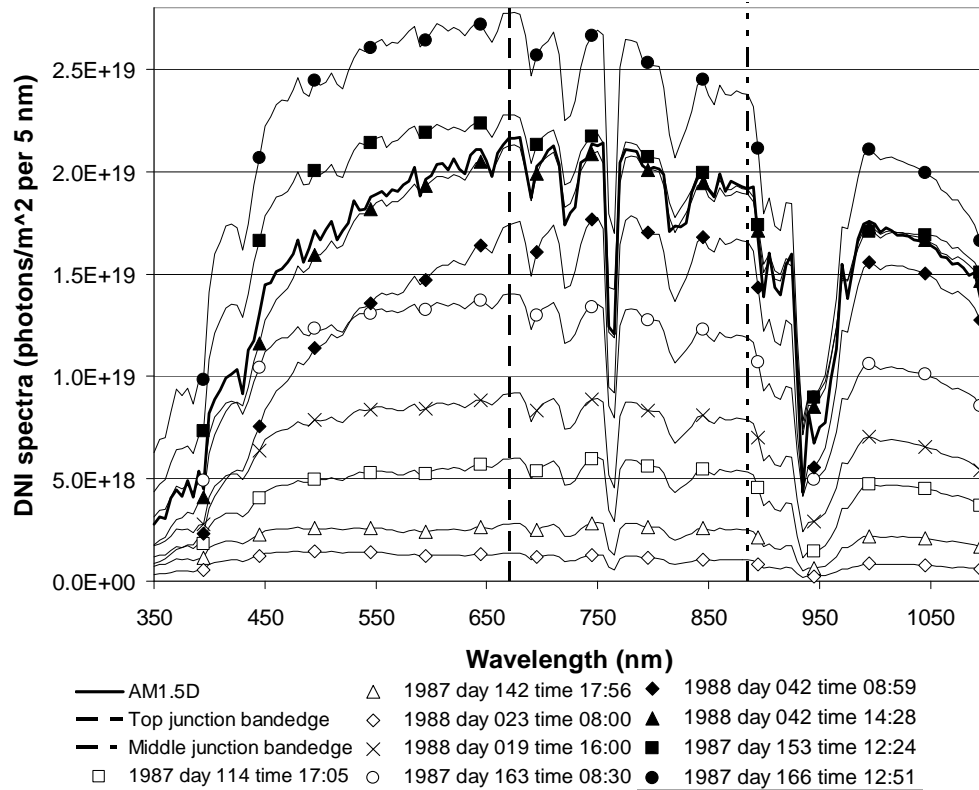


Figure 13 Sample DNI spectra from San Ramon, CA. Plain solid line is AM1.5D. The vertical dashed line depicts the band edge of the top junction, and the dash dot line that of the middle junction.

As remarked above, the AM1.5D spectrum is a rough average of the curves included in the training set; however, there are numerous occasions for which either the top junction or middle junction would gain disproportionately to DNI generally. For those occasions, a non-linear current constraint would occur and reduce system efficiency, an impairment that would not be predicted by using AM1.5D scaled linearly by DNI. The more general approach of using the full training set for optimization will include both the linear and non-linear response of the CPV system, include a sampling of typical weather conditions, and thereby obtain an accurate optimization of annual system energy collection.

We then simulated the performance of the system with a discrete set of AR filters. The result of that simulation is shown in Figure 14. The error in these FOM estimates could be determined by use of training sets drawn from other years; however, the SERI database used in this study was limited to data from a single year, so that approach is not straightforwardly applied. Based on the 0.4% standard deviation estimated (see section 2) in predicting current balance for a single spectrum, we can anticipate substantially smaller errors in predicting the mean annual energy FOM based on 250 independent spectra. If the spectral balance estimation errors are independent, the error in estimating the mean of the FOM would be <0.03%.

The potential value of an AR treatment for CPV is evident in that all simulations indicated a substantial increase annual energy production compared to a baseline system with a non-AR cover plate. To realize the greatest cost-effectiveness, one should choose the AR peak wavelength such that the figure of merit is maximized. Were AM1.5D used for system optimization, the system figure of merit would be maximized for an AR peak wavelength of ~525 nm. For San Ramon, CA training set, the system figure of merit would be maximized for an AR peak wavelength of ~625 nm. For the Cape Canaveral, FL training set, the system figure of merit would be maximized for an AR peak wavelength of ~600 nm. Assuming that the training set is more representative of the installation site, spectral optimization based on AM1.5D would result in overestimating potential gains by ~0.5% on an absolute scale. More

important, optimization based on AM1.5D alone would result in system underperformance of ~0.25% and ~0.5% compared to optimization based on site specific spectral data.

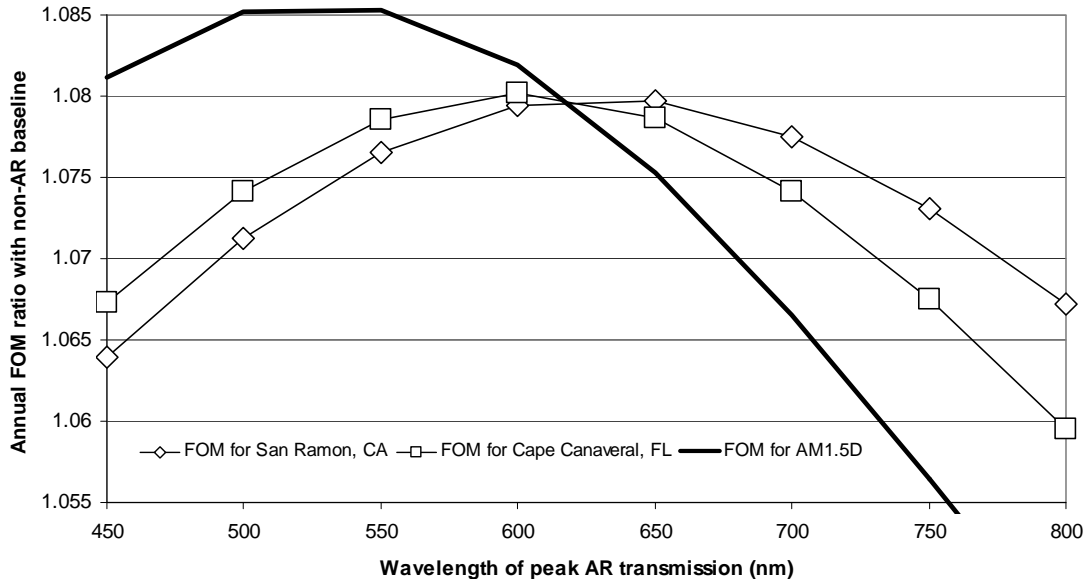


Figure 14 System figure of merit for various AR peak frequencies

5. CONCLUSIONS

We have constructed a system model based on a spectral transfer function that incorporates the essential performance of the SolFocus CPV optical system and commercial MJ cells. Using three independent methods, we have validated the model capability of predicting spectral balance of the top and middle junctions of commercial MJ cells. We find that condition of spectral balance can be predicted to better than 1% for instantaneous operating conditions of interest. Comparing optimization results based on AM1.5D and site specific data, we find that annual system energy production can be increased by up to 0.5% by utilizing site specific spectra.

ACKNOWLEDGMENTS

SolFocus would like to acknowledge the contribution of isotype cell measurement from NREL, and experimental assistance from Steve Askins, Sean Taylor, Steve Horne and the whole of the SolFocus engineering team.

REFERENCES

1. Kinsey et al., "Towards Commercialization of Concentrator Multijunction Photovoltaic Modules," 2008 33rd IEEE Photovoltaic Specialists Conference
2. McDonald et al., "Concentrator design to minimize LCOE", Proceedings Vol. 6649, High and Low Concentration for Solar Electric Applications II, Martha Symko-Davies, Editors.
3. Hessenkemper, "Boundary conditions for solar glass production," 2008 Photon International 1st PV Glass Conference
4. Optical Glass Catalog, available for download at www.us.schott.com.
5. C1MJ_CDO-100 product data sheet, available for download at www.spectrolab.com
6. McMahon et al., "Daily Fill Factor Variation as a Diagnostic Probe of Multijunction Concentrator Systems during Outdoor Operation," SPIE Proceedings Vol. 6649, High and Low Concentration for Solar Electric Applications II, Martha Symko-Davies, Editors.
7. Peharz et al., "Spectrometric Outdoor Characterization of CPV Modules using Isotype Monitor Cells," 2008 33rd IEEE Photovoltaic Specialists Conference
8. http://www.centrosolarglas.de/englisch/02_products/, accessed on 06-23-2008.
9. http://www.nrel.gov/redec/solar_data.html